Atomic Nitrogen Encapsulated in Fullerenes: Effects of Cage Variations

Elke Dietel,[†] Andreas Hirsch,*[,†] Björn Pietzak,[‡] Markus Waiblinger,[‡] Klaus Lips,[§] Alois Weidinger,[‡] Andrea Gruss,[||] and Klaus-Peter Dinse[||]

Contribution from Organic Chemistry II, Universität Erlangen, Henkestrasse 42, D-91054 Erlangen, Germany, Hahn-Meitner Institut Berlin, Glienickerstrasse 100, D-14109 Berlin, Germany, Hahn-Meitner Institut Berlin, Rudower Chaussee 5, D-14109 Berlin, Germany, and Physical Chemistry III, TU Darmstadt, Petersenstrasse 20, D-64287 Darmstadt, Germany

Received November 2, 1998

Abstract: The synthesis and EPR spectroscopic investigations of a family of six endohedral fullerenes, namely, N@C_{60} (**1**), N@$C_{61}(COOC_2H_5)_2$ (**2**), N@$C_{66}(COOC_2H_5)_{12}$ (**3**), N@$C_{66}(COOC_2D_5)_{12}$ (**4**), N@$C_{61}(COOC_2D_5)_2$ (**5**), and N@C_{70} (**6**), containing atomic nitrogen in the $^4S_{3/2}$ ground state is described. The parent systems N@C_{60} (**1**) and N@C_{70} (**6**) were synthesized by nitrogen ion implantation. The syntheses of the C_{2v}-symmetric monoadducts **2** and **5** and the T_h symmetric hexaadducts **3** and **4** exhibiting well-defined cage distortions were accomplished via cyclopropanation with the corresponding malonates. With respect to these additions the reactivity of **1** is indistinguishable from that of empty C_{60}. The quartet electronic spin of the encapsulated N-atoms is a very sensitive probe for cage modifications. In the monoadducts **2** and **5** a permanent zero field splitting (ZFS) tensor with rigidly aligned axes was revealed reflecting the intrinsic droplet like cage distortion. In contrast, no fine structure due to intrinsic distortions was monitored in the ESR spectra of the highly symmetric hexaadducts **3** and **4**. In these cases only matrix-induced distortions of the cage lead to ZFS interactions. In solution fluctuations of the ZFS tensor are the major source of spin relaxation. The root-mean-square value of this collision-induced fluctuating ZFS interaction as estimated from relaxation data for N@C_{60} (**1**) and the hexaadduct **3** is in the range of the ZFS interaction measured for the monoadduct **2**.

Introduction

In the endohedral complex N@C_{60} (**1**) nitrogen is found in its atomic ground state ($^4S_{3/2}$) and is located in the center of the fullerene cage.[1,2] Due to the high symmetry of C_{60}, the endohedral guest is subjected to an isotropic environment. The nitrogen keeps the spherical symmetry of the free atom as was shown by EPR and ENDOR spectroscopy.[1,2] The fact that the encapsulated N-atom does not form covalent bonds with the fullerene cage can be explained with the inertness of the inner concave surface of C_{60} resulting from its rigid structure with pyramidalized sp^2-C-atoms.[3] On the basis of this finding we predicted that fullerenes in general should be ideal containers for reactive otherwise hardly accessible species such as radicals.[4] In this respect the question arose whether it is possible to systematically fine-tune the wave function of the encapsulated N by changing the symmetry, size, and nature of the surrounding fullerene or fullerene derivative. As a first example, we have shown in a recent short communication that a permanent distortion of the cage symmetry from I_h to C_{2v}, realized via exohedral derivatization of **(1)** with the formation of N@$C_{61}(COOC_2H_5)_2$ (**2**), gives rise to an additional fine structure in the EPR spectra.[5] This can be explained by the fact that because of the lower symmetry of the cage the degeneracy of the three singly occupied p-orbitals is removed leading to a nonvanishing zero field splitting (ZFS) interaction sensed by the quartet electronic spin. We now report in full experimental detail on the synthesis and spectroscopic investigation of a family of six endohedral fullerenes, namely, N@C_{60} (**1**), N@$C_{61}(COOC_2H_5)_2$ (**2**), N@$C_{66}(COOC_2H_5)_{12}$ (**3**), N@$C_{66}(COOC_2D_5)_{12}$ (**4**), N@$C_{61}(COOC_2D_5)_2$ (**5**), and N@C_{70} (**6**) containing atomic nitrogen. We report on the influence of the nature of the cage on the fine and hyperfine structure of the EPR spectra on the relaxation behavior of the paramagnetic nitrogen guest. The results of the EPR investigations are compared with those of quantum mechanical calculations.

Experimental Section

General Details. Commercially available C_{60} and C_{70} (grade 99.5+% and 98+%, respectively) were used as starting materials in these experiments. UV/vis spectra were recorded on a Shimadzu UV 3102 PC spectrometer. The preparative HPLC separation was carried out on the Shimadzu system: Sil 10 A, SPD 10 A, CBM 10 A, LC 8 A, FRC 10 A. As stationary phase Grom-Sil 100 Si, NP1, 5 μm, 250 × 20 mm was used. All addition reactions were carried out under nitrogen in dry solvents.

Syntheses. N@C_{60} (**1**) and N@C_{70} (**6**) were produced by nitrogen implantation.[1] Thereby, the fullerenes were evaporated from an effusion

[†] Universitat Erlangen.
[‡] Hahn-Meitner Institut Berlin, Glienickerstrasse 100.
[§] Hahn-Meitner Institut Berlin, Rudower Chaussee 5.
[||] TU Darmstadt.

(1) Almeida Murphy, T.; Pawlik, T.; Weidinger, A.; Höhne, M.; Alcala, R.; Spaeth, J. M. *Phys. Rev. Lett.* **1996**, *77*, 1075.
(2) Knapp, C.; Dinse, K.-P.; Pietzak, B.; Waiblinger, M.; Weidinger, A. *Chem. Phys. Lett.* **1997**, *272*, 433.
(3) Mauser, H.; Clark, T.; Hirsch, A.; Pietzak, B.; Weidinger, A.; Dunsch, L. *Angew. Chem.* **1997**, *109*, 2858; *Angew. Chem., Int. Ed. Engl.* **1997**, *36*, 2835.
(4) Mauser, H.; Hirsch, A.; Hommes, N.; Clark, T. *J. Mol. Mod.* **1997**, *3*, 415.
(5) Pietzak, B.; Waiblinger, M.; Almeida Murphy, T.; Weidinger, A.; Höhne, M.; Dietel, E.; Hirsch, A. *Chem. Phys. Lett.* **1997**, *279*, 259.

10.1021/ja983812s CCC: $18.00
Published on Web 03/05/1999

cell onto a copper substrate and simultaneously irradiated with nitrogen ions from an intense ion source. Typical values of the ion energy and the current were 40 eV and 50 μA, respectively. After several hours of production the irradiated material was removed from the copper substrate, dissolved in toluene, and filtered. Usually only 10−20% is soluble; the rest remains in the filter. The soluble fraction of typically 10−20 mg contains **1** in C_{60} or **6** in C_{70} in a concentration of the order of $10^{-4}-10^{-5}$.

Perdeuterated Diethyl Malonate. Pyridine (1.0 mL, 12.4 mmol) was added to a solution of ethanol-d_6 (0.7 mL, 12.2 mmol) in methylene chloride (5 mL). After the flask was cooled with an ice bath, malonyl chloride (546 μL, 5.6 mmol) was added dropwise, and the mixture was stirred at room temperature overnight. Water was then added, the organic layer was separated and washed with 0.1 M HCl and $NaHCO_3$ solutions, and the filtrate was dried ($MgSO_4$). The solvent was evaporated to give 371 mg of deuterated diethyl malonate (36%): ^{1}H NMR (400 MHz, $CDCl_3$) δ 3.36 (2 H, s, CH_2); MS *m*/*z* 170 (M^+), 120 ($M^+ - D_5C_2O$).

N@C_{61}($COOC_2H_5$)$_2$ (2).[5] A mixture of N@C_{60}/C_{60} (27.1 mg, 0.038 mmol), sodium hydride (8.9 mg, 0.37 mmol), and diethyl bromomalonate (9.6 μL, 0.056 mmol) was stirred in toluene (20 mL) for 6 h. The reaction was quenched with one drop of 2 N H_2SO_4. Column chromatography (silica gel, toluene/hexane 1/1) gave 10.5 mg of **2**/C_{61}($COOC_2H_5$)$_2$ (32%). The IR, NMR, and UV/vis spectroscopic data of this mixture of **2**/C_{61}($COOC_2H_5$)$_2$ as well as the chromatographic behavior are indistinguishable from that of C_{61}($COOC_2H_5$)$_2$.[6]

N@C_{61}($COOC_2D_5$)$_2$ (5). A mixture of N@C_{60}/C_{60} (25.0 mg, 0.035 mmol), DBU (8.0 μL, 0.054 mmol), deuterated diethyl malonate (10.0 mg, 0.059 mmol), and CBr_4 (15.5 mg, 0.047 mmol) was stirred in toluene (20 mL) for 6 h. After the reaction was quenched with one drop of 2 N H_2SO_4, column chromatography (silica gel, toluene/hexane 1/1) was carried to give 10.4 mg of **5**/C_{61}($COOC_2D_5$)$_2$ (34%). The chromatographic behavior of **5**/C_{61}($COOC_2D_5$)$_2$ and its UV/vis spectrum (CH_2Cl_2, λ_{max} = 258, 326, 427 nm) are the same as those of **2**/C_{61}-($COOC_2H_5$)$_2$.

N@C_{66}($COOC_2H_5$)$_{12}$ (3). A mixture of N@C_{60}/C_{60} (29.9 mg, 0.041 mmol) and 9,10-dimethylanthracene (DMA; 82.3 mg, 0.40 mmol) was stirred in toluene (40 mL) for 2 h. DBU (59.8 μL, 0.40 mmol) and diethyl bromomalonate (67.3 μL, 0.40 mmol) were added, and the solution was stirred for 45 h. The mixture of **3** and C_{66}($COOC_2H_5$)$_{12}$ was separated by flash chromatography (silica gel, toluene/ethyl acetate 90/10) followed by HPLC (Grom-Sil, toluene/ethyl acetate 90/10). Yield: 35% (HPLC). The IR, NMR, and UV/vis spectroscopic data of this mixture of **3**/C_{66}($COOC_2H_5$)$_{12}$ as well as the chromatographic behavior are indistinguishable from those of C_{66}($COOC_2H_5$)$_{12}$.[7]

N@C_{66}($COOC_2D_5$)$_{12}$ (4). A mixture of N@C_{60}/C_{60} (29.1 mg, 0.040 mmol) and DMA (85.5 mg, 0.42 mmol) was stirred in toluene (40 mL) for 2 h. Deuterated diethyl malonate (71.5 mg, 0.42 mmol), CBr_4 (138 mg, 0.42 mmol), and DBU (124.2 μL, 0.83 mmol) were added, and the solution was stirred for 45 h. After flash chromatography (silica gel, toluene/ethyl acetate 90/10), the mixture of **4**/C_{66}($COOC_2H_5$)$_{12}$ was purified by HPLC (Grom-Sil, toluene/ethyl acetate 90/10). Yield: 35% (HPLC). The chromatographic behavior of **4**/C_{66}($COOC_2D_5$)$_{12}$ and its UV/vis spectrum (CH_2Cl_2, λ_{max} =245, 270, 280, 317, 336 nm) are the same as those of **3**/C_{66}($COOC_2H_5$)$_{12}$.

EPR Spectroscopy. EPR spectra were recorded using commercial continuous wave and FT X-band spectrometers. All samples were studied in quartz tubes sealed-off under high-vacuum conditions.

Results and Discussion

(1) Synthesis of N@C_{70} and Exohedral Adducts of N@C_{60}. For the modification of the nature of the fullerene cage, such as changes of the cage size, cage symmetry, and electronic structure of the cage framework, two possibilities can be considered: (1) variation of the parent fullerene itself and (2) modification of the cage by exohedral derivatization. Since the exohedral chemistry of fullerenes, especially that of the most abundant and most symmetrical C_{60}, is now facing a mature state,[8] the latter strategy offers the advantages of the facile control of the great diversity of fullerene adducts with known geometry, symmetry and addition pattern. In addition, the nature of the addends can easily be varied allowing for the investigation of their potential interaction with the encapsulated N-atom.

The synthesis of N@C_{70} is accomplished essentially in the same way as the synthesis of N@C_{60}, i.e., by ion implantation. In the specific case a modified apparatus was used which consists of a glow discharge tube in an oven. In this simplified setup, the nitrogen ions are provided by the glow discharge and the fullerenes are continuously deposited on the cooled cathode where they are hit by the ions. For additional details, see ref 5.

As model reaction for the exohedral modification of the cage structure we used the nucleophilic cyclopropanation of the [6,6]-double bonds with malonates in the presence of base.[6,9] This reaction inter alia allows for an easy access to both C_{2v}-symmetric monoadducts and T_h-symmetric hexaadducts in good yields. For the monoadduct C_{61}($COOC_2H_5$)$_2$[10] and the hexaadduct C_{66}($COOC_2H_5$)$_{12}$,[11] the X-ray crystal structures are known which is very important for the analysis of the influence of the cage structure on the properties of the encapsulated N-atoms. The synthesis of the monoaduct **2** and the hexaadduct **3** is depicted in Scheme 1. To evaluate the influence of the H-atoms of the addends on the relaxation behavior of the encapsulated N-atoms, we synthesized the corresponding perdeuterated compounds **4** and **5** for comparison (Scheme 1). Hexaadducts such as T_h-C_{66}($COOEt$)$_{12}$ can be prepared by the template activation method that we developed previously.[9,11] In this one-pot reaction, 9,10-dimethylanthracene (DMA) is used for the activation of [6,6]-double bonds at octahedral sites. This method can be transferred to the synthesis of **3** and **4** which were isolated as mixtures with the corresponding empty hexaadducts as yellow solids.

Under such reaction and workup conditions, the encapsulated N-atoms are not attacked but completely shielded from the environment by their host, since the ratio of filled and unfilled material does not change during the reaction as was monitored by EPR. Apparently, there is no difference in reactivity between C_{60} and N@C_{60} with respect to functionalization.

(2) Effect of the Cage Size. In Figure 1 solution EPR spectra of N@C_{60} (**1**), hexaadduct **3**, and N@C_{70} (**6**) are represented for comparison. The three lines in each spectrum are due to the hyperfine interaction (hfi) of the unpaired electrons with the nuclear spin I = 1 of ^{14}N. An accurate determination of the hyperfine splitting using FT-EPR shows that the hfi of the hexaadduct **3** is 100(10) kHz smaller than that of **1**, corresponding to a relative shift of only 0.7%. Considering that the hyperfine interaction of **1** is about 50% larger than that of free nitrogen, this implies a minute shift toward the value of the free atom. This might be interpreted as being due to an increase of the inner space after the covalent binding with the resulting elongation of the six [6,6]-bonds in octahedral positions carrying the addends. Indeed, the analysis of the X-ray single-crystal structure of C_{66}($COOC_2H_5$)$_{12}$ reveals an enlargement of the interior compared to the parent C_{60}.[11] The distance between the centers of two opposite sp^3 [6,6]-bonds is 731 pm whereas the

(6) Bingel, C. *Chem. Ber.* **1993**, *126*, 1957.

(7) Hirsch, A.; Lamparth, I.; Grösser, Th.; Karfunkel, H. R. *J. Am. Chem. Soc.* **1994**, *116*, 9385.

(8) (a) Hirsch, A. *The Chemistry of the Fullerenes*; Thieme: Stuttgart, 1994. (b) Hirsch, A. *Synthesis* **1995**, 895. (c) Diederich, F.; Thilgen, C. *Science* **1996**, *217*, 317.

(9) Camps, X.; Hirsch, A. *J. Chem. Soc., Perkin Trans. 1* **1997**, 1595.

(10) Paulus, E. F.; Bingel, C. *Acta Crystallogr.* **1995**, *C 51*, 143.

(11) Lamparth, I.; Maichle-Mössmer, C.; Hirsch, A. *Angew. Chem.* **1995**, *107*, 1755; *Angew. Chem., Int. Ed. Engl.* **1995**, *34*, 1607.

Scheme 1. Synthesis of $N@C_{61}((COOC_2H_5)_2$ (**2**), $N@C_{61}((COOC_2D_5)_2$ (**5**), $N@C_{66}((COOC_2H_5)_{12}$ (**3**), and $N@C_{66}((COOC_2D_5)_{12}$ (**4**)[a]

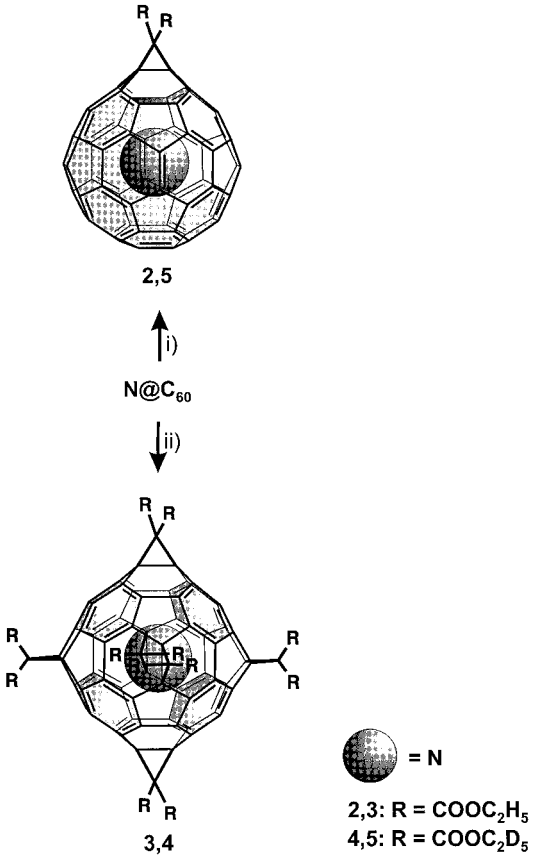

[a] Key: (i) diethyl bromomalonate, DBU, toluene, room temperature; (ii) diethyl bromomalonate, DBU/DMA, toluene, room temperature.

corresponding diameter in C_{60} is 696 pm. As in the case of $N@C_{60}$[2] (Figure 1a) no satellites due to ^{13}C coupling could be detected for the hexaadduct (Figure 1b) under the current spectral resolution of 1 μT.

The shift of the isotropic hyperfine splitting constant toward the value of the free N-atom is more pronounced upon going to the larger cage of C_{70}. In C_{70}, the distance between planes of two pentagonal end faces is 780 pm, the diameter of the equator is 699 pm, this dimension being practically identical to the C_{60} diameter.[12] In **6** the value of the coupling constant is reduced by 735(10) kHz, approximately 5% compared to **1** (Figure 1c**).** Pulsed EPR data revealed that the homogeneous line width of **6** is also remarkably narrow ($\Delta\nu$ (fwhm) = 8 kHz), but it is nevertheless somewhat larger than that of **1** for which $\Delta\nu$ (fwhm) = 2.5 kHz was measured under identical conditions. The influence of the nonvanishing ZFS tensor in $N@C_{70}$ might be the reason for this increase.

(3) Influence of the Cage Symmetry. Figure 2 shows the solid-state EPR spectra of $N@C_{60}$ (**1**), the deuterated monoadduct **5**, and the deuterated hexaadduct **4.** The data are presented on an extended vertical scale in order to emphasize the additional structures present in the spectra besides the main triplet structure already known from the solution spectra of Figure 1. The additional structure is most pronounced for the monoadduct (Figure 2b) and can be explained (see fit curve, solid line) by a fine structure interaction with D = 6.1 MHz and E = 0.45 MHz. This fine structure is already known from the corresponding hydrogenated monoadduct **2** (ref 5), but for the deuterated species **5** shown here, the details are better visible since the line widths are smaller. The appearance of a fine structure is a clear signature for a nonspherical electron distribution of the encapsulated nitrogen atom. The fact that the asymmetry parameter E is unequal zero indicates that the distortion is nonaxial symmetric, consistent with the known symmetry of

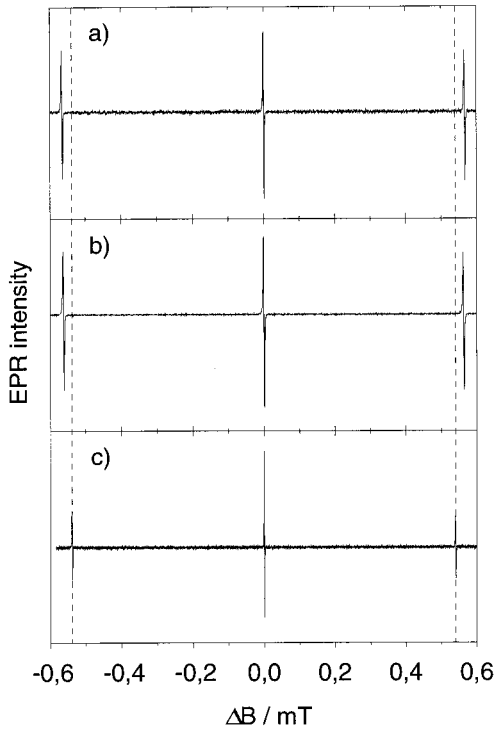

Figure 1. EPR spectra (X-band) of $N@C_{60}$ (**1**) (top), $N@C_{66}(COOC_2H_5)_{12}$ (**2**) (middle), and $N@C_{70}$ (**6**) (bottom) in solution. The horizontal dashed line is a guide to the eye to visualize the change of nitrogen hfi.

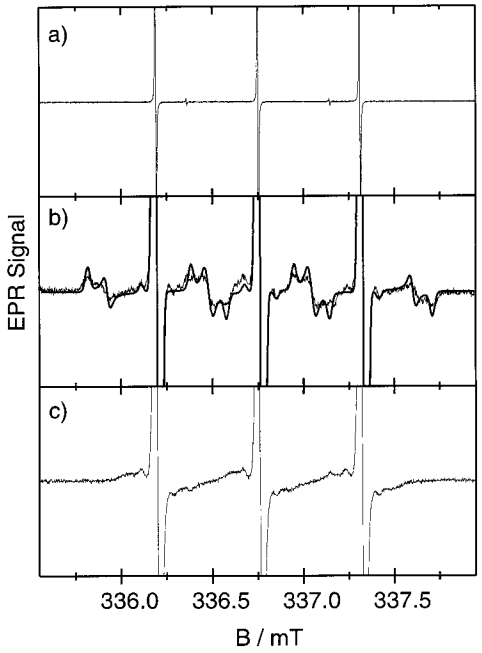

Figure 2. Powder EPR spectra of (a) $N@C_{60}$ **(1)**, (b) $N@C_{61}(COOC_2D_5)_2$ (**5**), and (c) $N@C_{66}(COOC_2D_5)_{12}$ (**4**). The solid line in Figure 2b is calculated assuming a fine structure interaction with D_{zz} = 6.1 MHz and E = 0.45 MHz. The line widths extracted from the data are given in Table 1.

(12) McKenzie, D. R.; Davis, C. A.; Cockayne, D. J. H.; Muller, D. A.; Vasallo, A. M. *Nature* **1992,** *355,* 622.

the monoadduct cage which is only C_{2v}.[10] For pure N@C_{60} (**1**) and for the hexaadduct (**4**) (Figure 2a and c, respectively), no such fine structure is observed, the additional features seen in these spectra are of a different origin. The two weak lines in the upper spectrum belong to N@C_{60} with the isotope ^{15}N, which is present in the N_2 gas with a natural abundance of 0.37%. The weak satellites on the left and the right of each line in the lower spectrum (Figure 2c) are tentatively assigned to spin-flips of the deuteron nuclei in the addends and are not connected with symmetry properties of the system. The broad structure below each line in the Figure 2c will be discussed below. Thus, the conclusion from these data is that the monoadduct **5** shows a fine structure and therefore is not spherical symmetric, whereas nitrogen in pure N@C_{60} (**1**) and in the hexaadduct **4** keeps its spherical electron distribution.

In **5** and **2** the three singly occupied p-orbitals of N-atom are no longer degenerate.[5] In the hexaadducts, however, the cage symmetry is lowered only to T_h. Semiempirical calculations (PM3/UHF)[13] performed on the model compound N@$C_{66}H_{12}$[14] with T_h symmetry confirm the experimental results (Figure 3): (i) In the most stable structure the N-atom is in its quartet state and is located in the center of the cage. (ii) There is no charge transfer between host and guest. The Mulliken partial charge on N is zero. The spin density is exclusively located on the N-atom. (iii) The three singly occupied orbitals of the N@$C_{66}H_{12}$ system are degenerate ($E = -13.773$ eV, $\Delta E < 0.001$) and N-centered (p-orbitals). An analogous situation arises for **1** ($E = -14.691$ eV, $\Delta E < 0.001$), whereas in **5** the three singly occupied orbitals are no longer degenerate ($E_{p_x} = -14.739$ eV, $E_{p_y} = -14.742$ eV, $E_{p_z} = -14.743$ eV).[5]

Assuming that the N-atom is still located in the cage center, no ZFS can exist for the quartet spin because the three p-orbitals stay degenerate. Therefore, equal occupation of the p-orbitals with one electron each results in a spherical electron distribution, and consequently, no fine structure splitting arises.

(4) Dipolar Interaction with the Protons and Deuterons of the Exohedral Addends. To explain the increase in line width observed for the adducts in the solid matrix, two possibilities had to be considered. First, hyperfine interaction of the central quartet electronic spin with the protons of the addends can lead to inhomogeneous line broadening, and second, matrix-induced cage distortions might result in a distribution of nonvanishing ZFS parameters. Here it should be noted that the site symmetry of **3** and **4** as revealed by the X-ray data is only *I*, thus causing in principle the existence of a finite ZFS in the crystalline matrix.

We discriminated between these possibilities by synthesizing the deuterated adducts **5** and **4** in analogy to the hydrogenated adducts **2** and **3**. Indeed, the perdeuteration causes a reduction of the line width measured in the powder as can be seen in Figure 4 and Table 1. The theoretical value for the ratio of the line width between the hydrogenated and the deuterated species is 4.0, in fair agreement with the value found for the hexaaduct but somewhat off for the monoadduct. An explanation for the deviation in case of the monoadduct might be that additional contributions to the line width increase the value of the deuterated monoadduct. The general increase of the width from the mono- to the hexaadducts (Table 1) can be attributed to the number of nearby hydrogens and deuterons increasing with the number of addends. In a simple model considering only the contribution from the local addends of each molecule, the ratio between the width of the hexa- and monoadduct should be $\sqrt{6}$. The observed values (Table 1) are smaller. This can be rationalized since the contributions of the addends of the neighboring molecules are more significant in case of the monothan in case of the hexaadduct. In any case, the observed isotope effect on the powder EPR line widths can be taken as evidence that the line broadening is caused mainly by anisotropic electron−nuclear dipole−dipole interactions. These have to be traceless, because in solution no isotropic terms are observed.

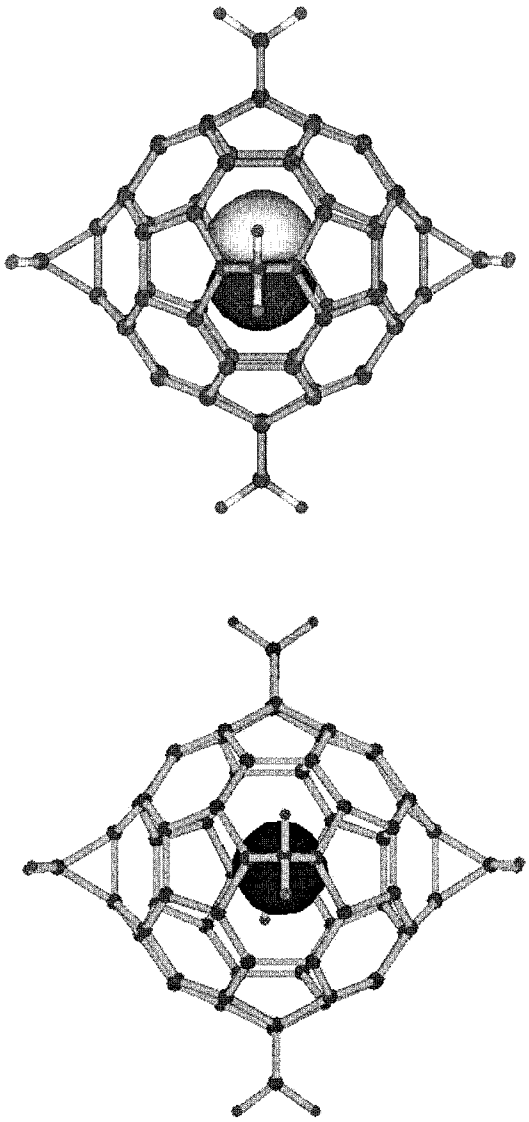

Figure 3. One of the three degenerate p-orbitals (top) and spin density of the T_h-symmetrical hexaadduct $C_{66}H_{12}$ obtained from a semiempirical PM3 calculation.

(5) Crystal Field Effects. To determine if an additional small ZFS might be induced by a crystal field of low symmetry, we compared the EPR spectrum of the totally deuterated hexaadduct **4** with that of the parent compound **1**. Indeed, a small matrix effect, i.e., symmetry lowering of the cage caused by the crystal field or by crystal imperfections, could be observed by invoking electron spin−echo (ESE) detection techniques or by Fourier transforming the electron spin−echo. Line broadening, as caused by modulation and/or saturation in continuous wave EPR is avoided and by the latter method also broadening by nonselective excitation is excluded, thus allowing for a distortion-free observation of spectra with superimposed broad and narrow lines.

(13) *HyperChem 5.0*; Hypercube, Inc.: Waterloo, Ontario, N2L 2 × 2, Canada, 1997.

(14) To reduce CPU time and to avoid problems with local minima arising from different conformations of the addends, the ethoxy carbonyl groups were replaced by H-atoms for the semiempirical calculations.

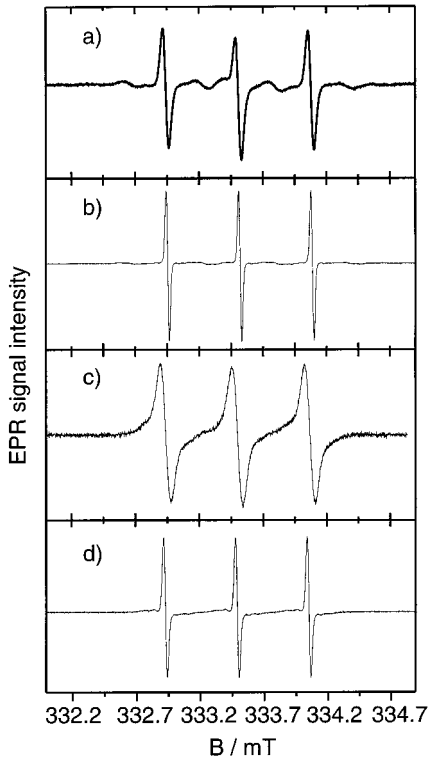

Figure 4. Powder EPR spectra of (a) N@C_{61}(COO C_2H_5)$_2$ (**2**), (b) N@C_{61}($COOC_2D_5$)$_2$ (**5**), (c) N@C_{66}($COOC_2H_5$)$_{12}$ (**3**), and (d) N@C_{66}-($COOC_2D_5$)$_{12}$ (**4**).

Table 1. Experimental Values of Continuous Wave EPR Line Width (peak-to-peak) for Hydrogenated and Deuterated Mono- and Hexaadducts

exptl	monoadduct	hexaadduct	ratio hexa/mono
H	47 μT	85 μT	1.8
D	17 μT	23 μT	1.4
ratio H/D	2.8	3.7	

Figure 5 shows the absorption mode powder EPR spectra of compounds **4** and **1**. Clearly resolved additional lines, which were observed in the monoadduct spectrum, are missing in the hexaadduct as well as in the N@C_{60} sample. As is seen in Figure 5, in **4** three narrow lines (although somewhat broadened by unresolved deuteron hfi) reside on a broad structure, indicating that the high molecular symmetry at the nitrogen site is lifted. Apparently, this leads to a distribution of ZFS values ranging from $|D| = 0$ to 7 MHz, estimated from the edges of the broad "feet" in the EPR spectrum (Figure 5). To exclude experimental artifacts which could lead to similar features, a spectrum of **1** under the same experimental conditions was recorded. Matrix-induced distortions should vanish in the solid phase of **1**, because fast molecular tumbling of C_{60} at room temperature leads to an averaged D value of zero. Indeed, no cage deformation could be detected for N@C_{60}.

The line shape differences of **4** and **1** are more pronounced in the time domain data, measured with a two-pulse spin−echo. Figure 5 shows spin−echoes obtained by selectively exciting the high field hfi transitions. In **4**, the narrow "spike" residing on a broader echo is characteristic for the existence of the "broad foot" in the frequency domain, indicating a nonvanishing ZFS. The amplitudes of the spike and the broader component are nearly equal, proving that all molecules are influenced by the crystal-field-derived deformation. The very broad echo of **1** is characteristic for the extremely narrow line of N@C_{60}.

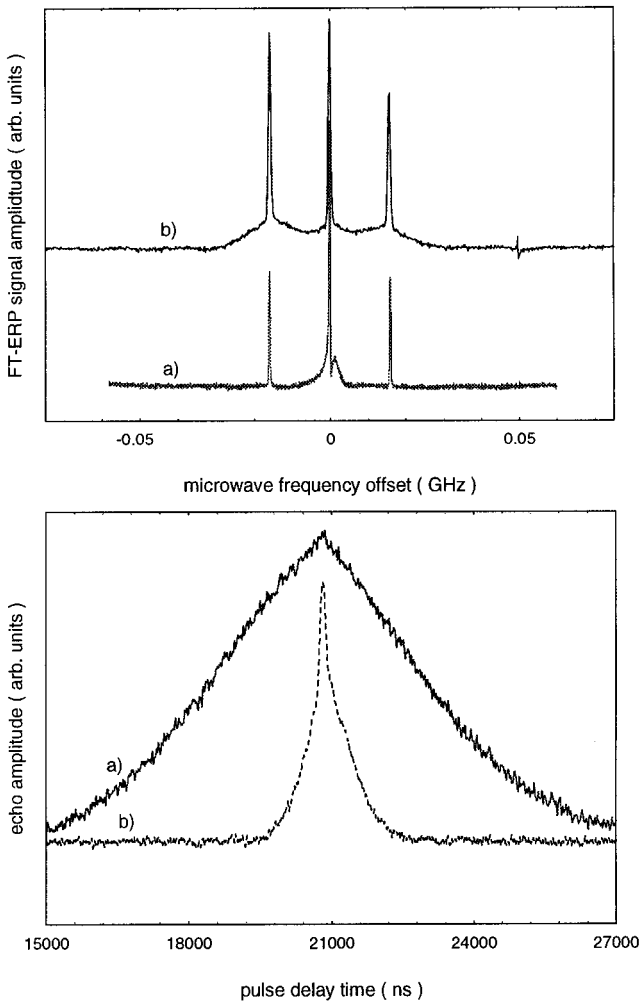

Figure 5. (Top) Echo-transformed powder spectra of (a) I_h-N@C_{60} (**1**) and (b) perdeuterated T_h-N@C_{66}($COOC_2D_5$)$_{12}$ (**4**). (Bottom) Two-pulse spin−echoes of (a) I_h-N@C_{60} (**1**) and (b) perdeuterated T_h-N@C_{66}-($COOC_2D_5$)$_{12}$ (**4**).

Table 2. Spin Relaxation Times Measured at 300 K, Correlation Times of the ZFS Interactions, and Permanent Respectively Temporary Effective D Values for Nitrogen Encapsulated in Cages of Different Symmetry. a) Toluene Solution, b) Dichloromethane Solution, c) CS_2 Solution

	N@C_{61}-($COOC_2H_5$)$_2$[a]	N@C_{66}-($COOC_2H_5$)$_{12}$[b]	N@C_{60}[a]	N@C_{70}[b]
T_2 [μs]	13(2)	24(2)	50(1)	40(5)
T_1 [μs]	78(5)	116(3)	120(2)	133(5)
τ [ps]	25	20	11	15
$\lvert D_{\text{eff}}\rvert$ [MHz]	8.5	6.8	5.8	6.0

(6) Molecular Dynamics of the Various Complexes in Solution. The special position of the nitrogen in the symmetrical cage is responsible for exceptional long spin relaxation times of N@C_{60},[2] because most of the mechanisms otherwise causing electronic spin transitions, e.g., ZFS interaction, anisotropy of the g matrix and of the electron−nuclear dipole interaction, and the nuclear quadrupole interaction, are absent if the nitrogen atom is located at the center of the C_{60} shell. In addition, spin rotational interaction is also suppressed if the electronic spin is confined to the N-atom. We measured the electron spin relaxation times T_1 and T_2 for **1** and for two of its adducts by the inversion recovery method and by spin−echo experiments, respectively (see Table 2).

For an analysis, we assumed that lowering of the site symmetry, either by cage distortions induced by collisions with the solvent molecules or by functionalization or by placing the N-atom in a fullerene of lower cage symmetry, is a prerequisite for spin relaxation. Assuming further that ZFS interaction is the leading term in the time-dependent part of the spin Hamiltonian, spin relaxation times can be approximated by[15]

$$\frac{T_1}{T_2} = {}^1/_2 \frac{\tau + \tau/(1+\omega^2\tau^2)}{\tau/(1+4\omega^2\tau^2)} \quad (1)$$

$$\frac{1}{T_1} \approx {}^8/_5(D^2+3E^2)\frac{\tau}{1+4\omega^2\tau^2} \quad (2)$$

The principal values of the ZFS interaction and the electron Zeeman frequency are denoted by D and E, and by ω, respectively (all values given in angular frequency units). The correlation time τ describes the orientation change of the principal ZFS axis, which is either controlled by rotational tumbling or by fluctuating impact sites on the cage. The given expressions are both approximate, because ideally two different decay modes for T_1 and T_2 would be expected.[16] Attempts to deconvolute the observed decay curves into two exponentials were not successful, however, probably because of the limited signal-to-noise ratio of the data and because predicted time constants are very similar in the expected range of $\omega\tau$.

The monoadduct with its molecular frame-fixed ZFS tensor was invoked for a test of the applicability of the above approximations. Evaluation of the room-temperature data measured in toluene lead to a rotational correlation time of 25 ps and a value for $|D_{\text{eff}}| = 8.5$ MHz ($D_{\text{eff}} = \sqrt{(D^2+3E^2)}$; D and E were evaluated independently by an analysis of the rigid limit powder spectrum of the same compound (see below), resulting in $D_{\text{eff}} = 6.1$ MHz (see Figure 2b). This close coincidence indicates that modulation of the permanent ZFS by rotational tumbling is the major source of spin relaxation in solution for this compound. Furthermore, the value deduced for τ, which is significantly larger than the rotational correlation time of unmodified C_{60}, is in agreement with values estimated by a classical Stokes/Einstein relation for rotational diffusion controlled by the attached group.

In the absence of a permanent cage distortion, as is the case of unmodified N@C_{60} or of its hexaadduct, a ZFS tensor rigidly attached to the molecular frame is lacking and therefore rotational tumbling cannot induce spin relaxation. Instead, we have to consider collision-induced deformations of the carbon shell leading to a temporary ZFS tensor fluctuating in direction and magnitude.[16] Table 2 summarizes the experimental data for T_1 and T_2 and the correlation times τ of the interaction as well as the resulting effective ZFS parameter $|D_{\text{eff}}|$.

It can be seen that the value of the effective zero field splitting $|D_{\text{eff}}|$ is only slightly larger for the permanently deformed monoadduct than for the symmetrical N@C_{60} and the hexaadduct, indicating that the ZFS interaction resulting from the permanent deformation of the monoadduct and the root-mean-square average of collision-induced cage deformations in solution are of the same order of magnitude.

N@C_{70} with its D_{5h} cage symmetry does not provide a site of cubic symmetry for the N-atom at any internal position. Spin relaxation therefore will be induced by a nonvanishing ZFS tensor modulated by rotational tumbling and also possibly by internal motion of the encased atom as well as by collision-induce deformations. The almost identical values of $|D_{\text{eff}}|$ for **1** and **6** imply that the ZFS contribution originating from the axial symmetry of the C_{70} cage is small compared to that from the collision-induced deformations in solution.

The correlation times τ are in the order of 10^{-11} s indicating fast changes of the direction of the principal ZFS axis. For the monoadduct with its molecular-fixed ZFS tensor, this corresponds to rotational tumbling; for symmetric molecules, it refers to the times between impacts. It is remarkable that the "bulky" hexaadduct does not differ much in its relaxation properties from the parent compound. The increase of τ from 11 to 20 ps might be interpreted as resulting from a decreased accessibility of the cage as a result of "screening" by the bulky addends. The trend of τ being shortest for N@C_{60} and increasing via N@C_{70} and the hexaadduct toward the monoadduct is plausible considering easiness of rotation and accessibility for impacts for these molecules in solution.

Conclusion

This work demonstrates that a multiple functionalization of the cage of N@C_{60} is possible without destroying the endohedral system. The N-atom is only an observer during these reactions but does not interact. Modifications of the cage structure by exohedral additions are therefore an unprecedented method for tuning the wave functions of nearly free atoms. Further investigations will deal with the question up to which extent the fullerene cage can be distorted without changing the atomic nature of the encapsulated N-atoms and how these distortions determine the atomic configuration and the thermal stability of the endohedral complexes.[3] The results of this work lead to the following conclusions: (i) In all endohedral complexes **1**−**6** investigated the nitrogen is present in its $^4S_{3/2}$ ground state and does not bind covalently with the fullerene cage. (ii) Only a small amount of spin density is transferred to the fullerene cage or to the addends, since no ^{13}C or ^1H couplings are observed within the spectral resolution obtained to date. (iii) Evaluation of the electron spin relaxation data in solution and the analysis of powder spectra reveal the existence of a permanent ZFS tensor with axes rigidly attached to the molecular frame for the monoadduct, which indicates an *intrinsic* distortion of the cage. In contrast, the distribution of ZFS interactions monitored by nitrogen in the hexaadduct are of *extrinsic* nature and can be explained by matrix-induced distortions of the cage. In solution, in the absence of a permanent ZFS interaction, fluctuations of the ZFS tensor are the major source of spin relaxation. The root-mean-square value of this collision-induced fluctuating ZFS interaction as estimated from relaxation data for N@C_{60}, and the hexaadduct is in the range of the ZFS interaction measured for the monoadduct. These investigations complement the work of Saunders and co-workers[17] where ^3He encapsulated by various fullerenes and exohedral fullerene adducts was used to probe the influence of the nature of the fullerene cage on the magnetic shielding within the cage.

Acknowledgment. We thank the Bundesminister für Bildung, Wissenschaft, Forschung und Technologie (BMBF) for financial support. We also gratefully acknowledge financial support from the Deutsche Forschungsgemeinschaft (Di182/19-1).

JA983812S

(15) Knapp, C.; Weiden, N.; Dinse, K.-P. *Appl. Phys. A* **1998**, *66*, 249.
(16) Rubinstein, M., Baram, A., Luz, Z. *Mol. Phys.* **1971**, *20*, 67.
(17) For example, see: (a) Saunders, M.; Cross, R. J.; Jimenez-Vazquez, A.; Shimshi, R.; Khong, A. *Science* **1996**, *271*, 1693. (b) Rüttimann, M.; Haldimann, R. F.; Isaacs, L.; Diederich, F.; Khong, A.; Jimenez-Vazquez, H.; Cross, R. J.; Saunders, M. *Chem. Eur. J.* **1997**, *3*, 1071. (c) Shabtai, E.; Weitz, A.; Haddon, R. C.; Hoffman, R. E.; Rabinovitz, M.; Khong, A.; Cross, R. J.; Saunders, M.; Cheng, P. C.; Scott, L. T. *J. Am. Chem. Soc.* **1998**, *120*, 6389.